Exfoliation of Graphite into Graphene in Aqueous Solutions of Inorganic Salts

Khaled Parvez,[†] Zhong-Shuai Wu,[†] Rongjin Li,[†] Xianjie Liu,[‡] Robert Graf,[†] Xinliang Feng,*,[†,§] and Klaus Müllen*,[†]

[†]Max Planck Institute for Polymer Research, Ackermannweg 10, Mainz 55128, Germany

[‡]Department of Physics, Chemistry, and Biology, Linköping University, Linköping SE-58183, Sweden

[§]School of Chemistry and Chemical Engineering, Shanghai Jiao Tong University, Shanghai 200240, P. R. China

Ⓢ *Supporting Information*

ABSTRACT: Mass production of high-quality graphene sheets is essential for their practical application in electronics, optoelectronics, composite materials, and energy-storage devices. Here we report a prompt electrochemical exfoliation of graphene sheets into aqueous solutions of different inorganic salts $((NH_4)_2SO_4$, Na_2SO_4, K_2SO_4, etc.). Exfoliation in these electrolytes leads to graphene with a high yield (>85%, ≤3 layers), large lateral size (up to 44 μm), low oxidation degree (a C/O ratio of 17.2), and a remarkable hole mobility of 310 cm^2 V^{-1} s^{-1}. Further, highly conductive graphene films (11 Ω sq^{-1}) are readily fabricated on an A4-size paper by applying brush painting of a concentrated graphene ink (10 mg mL^{-1}, in N,N'-dimethylformamide). All-solid-state flexible supercapacitors manufactured on the basis of such graphene films deliver a high area capacitance of 11.3 mF cm^{-2} and an excellent rate capability of 5000 mV s^{-1}. The described electrochemical exfoliation shows great promise for the industrial-scale synthesis of high-quality graphene for numerous advanced applications.
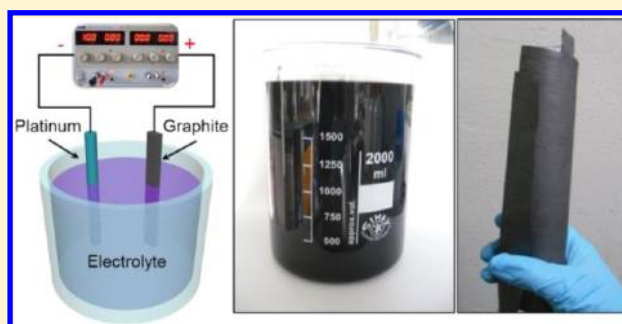
■ INTRODUCTION

Graphene, a two-dimensional honeycomb sp^2 carbon lattice, has received immense attention for its potential application in next-generation electronic devices,[1,2] composite materials,[3,4] energy storage devices,[5] etc. due to its intriguing electrical, mechanical, and chemical properties.[6,7] Mass production of high-quality, solution-processable graphene via a simple low-cost method, however, remains a major challenge. Several graphene preparation methods have been developed since its discovery.[8] Among them, mechanically exfoliated and epitaxially grown graphene provides high-quality material, but in only limited quantities, for fundamental research.[8,9] Chemical vapor deposition (CVD) using catalytic metal substrates such as Ni or Cu produces large-area high-quality graphene.[9,10] The major obstacles to cost-effective industrial-scale production of CVD-grown graphene, however, are the requirements of high temperature, a sacrificial metal, and multistep transfer processes onto the desired substrates. Chemical exfoliation of graphite based on the Hummers method is an appealing route to produce solution-processable graphene oxide (GO) in bulk scale but requires thermal or chemical reduction to partially restore the electronic properties of graphene.[11] Several other methods have been developed to overcome these limitations, such as solvent- and/or surfactant-assisted liquid-phase exfoliation,[12] electrochemical expansion,[13] and formation of graphite intercalated compounds.[14] Nevertheless, extensive

sonication processes are indispensable for these methods, which limit the size and yield of thin graphene layers.

Recently, electrochemical exfoliation of graphite has attracted attention due to its easy, fast, and environmentally friendly nature to produce high-quality graphene.[15−18] Electrochemical exfoliation of graphite has been performed mainly in two different types of electrolytes, i.e., ionic liquids[17,19] and aqueous acids (e.g., H_2SO_4 or H_3PO_4).[15,18,20] Exfoliation in ionic liquids results in only a low yield of graphene with a small lateral size (<5 μm) and often functionalize with the ionic liquids, which disrupt the electronic properties of graphene.[17,21] On the other hand, exfoliation in acidic electrolytes can yield graphene with a better quality and a larger lateral size, but a significant amount of oxygen-containing functional groups cannot be avoided due to the overoxidation of graphite by the acid.[15,18,20] Therefore, a proper electrolyte system that can balance the high-quality and large-quantity synthesis of exfoliated graphene (EG) is highly in demand.

In this work, we demonstrate a highly efficient electrochemical exfoliation of graphite in aqueous inorganic salts, such as ammonium sulfate $((NH_4)_2SO_4)$, sodium sulfate (Na_2SO_4), and potassium sulfate (K_2SO_4). Under neutral pH conditions for electrochemical exfoliation, graphene sheets with the

highest C/O ratio of 17.2 (i.e., oxygen content of 5.5 atomic % [atom %]) and lowest defect density were obtained. The EG sheets were readily produced on a scale of tens of grams, with ~80% of the flakes larger than 5 μm and ~85% of flakes having 1–3 layers. Moreover, single-layer graphene sheets had a high hole mobility of 310 cm^2 V^{-1} s^{-1} with a sheet resistance of 1.96 kΩ sq^{-1}, which is superior to the chemically reduced graphene oxide (rGO). The high solution-processability of EG further allowed for the preparation of concentrated graphene ink in N,N'-dimethylformamide (DMF) without any additional surfactants. A simple paintbrush application of EG-ink to A4-sized paper yielded highly conductive (~11 Ω sq^{-1} with 0.74 mg cm^{-2} EG loading), mechanically stable, and large-area graphene films. All-solid-state flexible supercapacitors fabricated on the basis of such graphene paper exhibited a high-area capacity of 11.3 mF cm^{-2} (at a scan rate of 1 mV s^{-1}) and a high rate capability (up to 5000 mV s^{-1}).

■ RESULTS AND DISCUSSION

Graphene Preparation by Electrochemical Exfoliation. Electrochemical exfoliation of graphite was performed in a two-
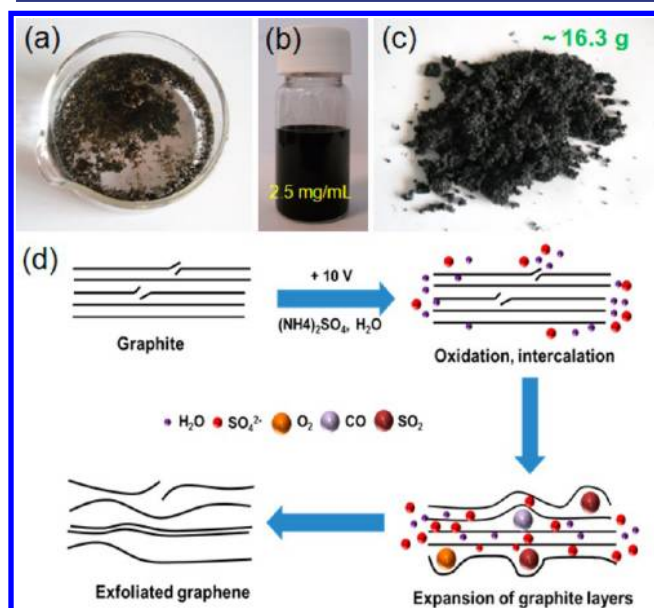
Figure 1. Photograph of (a) graphite flakes after electrochemical exfoliation, (b) dispersed EG in DMF solution (concentration ~2.5 mg mL^{-1}), (c) EG powders on a bulk scale (~16.3 g). (d) Schematic illustration of the mechanism of electrochemical exfoliation.

electrode system using platinum as the counter electrode and a graphite flake as the working electrode. Different types of aqueous inorganic salt electrolyte solutions were examined, and among them sulfate-containing salts such as $(NH_4)_2SO_4$ exhibited the best exfoliation efficiency. Electrolyte solutions were prepared by dissolving $(NH_4)_2SO_4$ in water (concentration of 0.1 M and pH ~6.5–7.0). When a direct current (DC) voltage of +10 V was applied to a graphite electrode, the graphite flakes began to dissociate and disperse into the electrolyte solution (Figure 1a). The voltage was kept constant for 3–5 min to complete the exfoliation process. Afterward, the exfoliated product was collected by vacuum filtration and repeatedly washed with water to remove any residual salts. The yield of the exfoliated EG flakes was more than 75% relative to the total weight of the starting graphite electrode. The collected

powder was then dispersed in DMF by sonication for 10 min. Thus, a dispersion of ~2.5 mg mL^{-1} was obtained, which was stable for 3 weeks without apparent agglomeration (Figure 1b). Remarkably, the exfoliation process could be readily scaled up depending on the type and size of the graphite electrode used (Supplementary Figure S1). For example, in a series of electrochemical experiments, ~16.3 g of graphene sheets was obtained (Figure 1c) within 30 min using three graphite foils (each with a dimension of 11.5 cm × 2.5 cm) simultaneously (Supplementary Figure S1a).

In addition to $(NH_4)_2SO_4$, various aqueous electrolyte solutions of inorganic salts, such as NH$_4$Cl, Na$_2$SO$_4$, NaNO$_3$, K$_2$SO$_4$, and NaClO$_4$, were examined in the electrochemical exfoliation process (see Supplementary Figures S2 and S3 and Table S1 for details). Salts containing anions, such as ClO$_4^-$, Cl$^-$, and NO$_3^-$, had no apparent exfoliation effects. Expansion of the graphite electrode was only observed when using ClO$_4^-$ and NO$_3^-$ anions. In contrast, salts containing sulfate anions (e.g., SO$_4^{2-}$) exhibited pronounced exfoliation efficiency. Thin graphene sheets were readily obtained in less than 5 min (Supplementary Figures S2d,e and S3). The superior exfoliation efficiency of sulfate salts compared to other anions can be attributed to the lower reduction potential of SO$_4^{2-}$ (+0.20 V) to generate SO$_2$ gas. In contrast, the reduction potential of ClO$_4^-$ and NO$_3^-$ ions to produce Cl$_2$ and NO gases is as high as 1.42 and 0.96 V, respectively (see Supplementary Scheme S1 for details).

We propose the mechanism of electrochemical exfoliation depicted in Figure 1d: (i) Applying bias voltage results in a reduction of water at the cathode, creating hydroxyl ions (OH$^-$) that act as a strong nucleophile in the electrolyte. The nucleophilic attack of graphite by OH$^-$ ions initially occurs at the edge sites and grain boundaries. (ii) Oxidation at the edge sites and grain boundaries then leads to depolarization and expansion of the graphite layers, thereby facilitating the intercalation of sulfate ions (SO$_4^{2-}$) within the graphitic layers. During this stage, water molecules may co-intercalate with the SO$_4^{2-}$ anions. (iii) Reduction of SO$_4^{2-}$ anions and self-oxidation of water produce gaseous species such as SO$_2$, O$_2$, and others, as evidenced by the vigorous gas evolution during the electrochemical process.[22,23] These gaseous species can exert large forces on the graphite layers, which are sufficient to separate weakly bonded graphite layers from one another.[24] This hypothesis was confirmed by controlled experiments in which a constant bias voltage (e.g., +10 V) was applied to graphite electrodes for different time periods (5–60 s) and changes in the morphology of the graphite foil were monitored by scanning electron microscopy (SEM) and optical microscopy. SEM images of both the surface and edge of the original graphite show closely packed layers (Figure 2a–c). When voltage was applied, however, the surface and edge morphology changed drastically within a few seconds (Supplementary Figure S4). After applying voltage for 5 s, the edge of the graphite foil expanded and the cracks in the graphite layers increased (Supplementary Figure S5b,c). When the time was increased from 5 to 60 s, a large amount of graphene flakes was exfoliated and dispersed into the electrolyte solution. After 60 s, the edge of the graphite foil expanded to almost 10 times that in the initial state (Figure 2b,h). Moreover, a network of ripples on the surface of the graphite was clearly identified in the SEM images (Figure 2d,g and Supplementary Figure S5a,d), which might be due to the visible gas evolution causing expansion and swelling of the graphite layers. These observations strongly
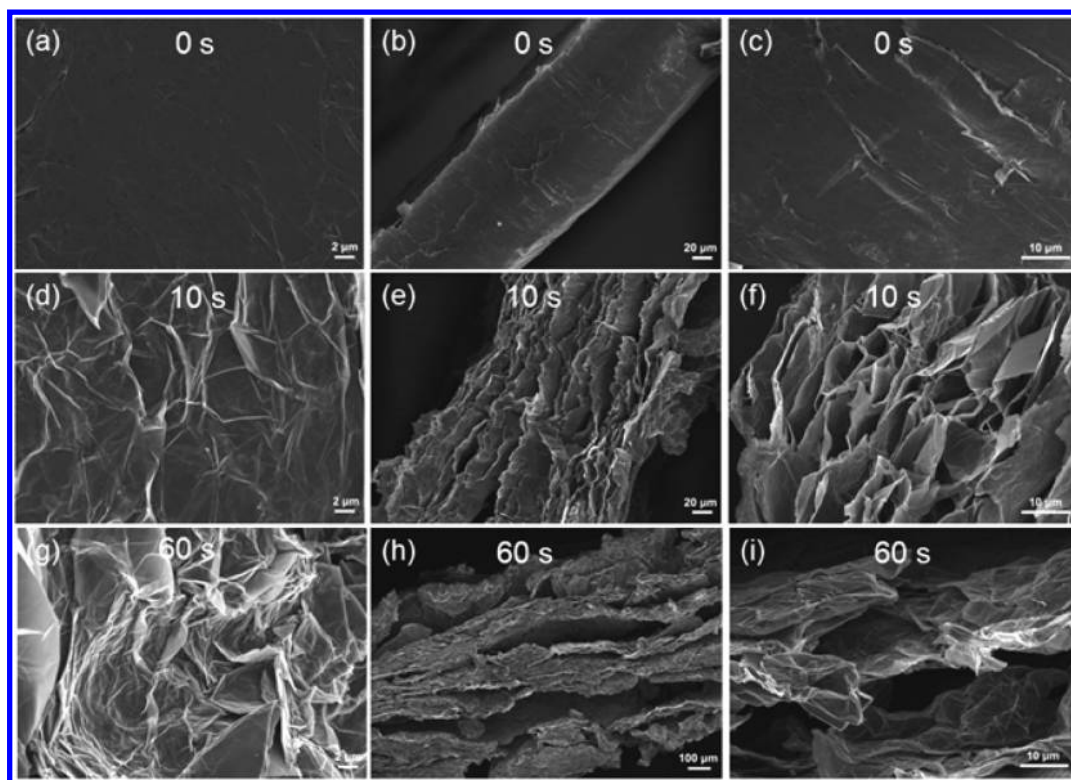
Figure 2. SEM images of (a,d,g) surface and (b,e,h) edge morphology of the graphite foil after applying a bias voltage of +10 V for 0, 10, and 60 s in aqueous $(NH_4)_2SO_4$ electrolyte solution, respectively. (c,f,i) Magnified images of panels b, e, and h, respectively.

support our hypothesis that during the electrochemical process, edge and grain boundaries of the graphite electrode open up first, which facilitates anion intercalation and results in exfoliated graphene sheets. A detailed reaction mechanism on the oxidation, i.e., oxide bond formation of graphite, is proposed and discussed in the Supporting Information (Scheme S2).

We further investigated the effect of the electrolyte concentration on the applied potential for graphite exfoliation. The voltage or potential for graphite exfoliation decreased upon increasing the concentration of $(NH_4)_2SO_4$ (Supplementary Figure S6a). When the concentration of $(NH_4)_2SO_4$ was lower than 0.01 M, the yield of EG was less than 5 wt %, indicating a limited amount of ions available for graphite intercalation. In sharp contrast, when the concentration increased from 0.01 to 1.0 M, a high yield of EG (>75 wt %) was obtained. A further increase in the concentration (e.g., 3.0 and 5.0 M), however, failed to enhance the graphene yield (<50%, Supplementary Figure S6b). As discussed above, the initial oxidation of graphite by OH^- ions at the edge and/or grain boundaries is essential for the depolarization and expansion of the graphite layers as well as for the following anion intercalation. With the high concentration of $(NH_4)_2SO_4$, the formation of OH^- ions is suppressed due to the low water content, and therefore the graphite edge oxidation, expansion, and SO_4^{2-} ion intercalation processes are expected to be relatively slow.

Morphological and Structural Characterizations of EG. The morphology of the EG sheets was investigated by SEM and atomic force microscopy (AFM). EG nanosheets were deposited on SiO_2 substrates using the Langmuir–Blodgett technique (Supplementary Figure S7a). Figure 3a shows a SEM image of a typical EG sheet (18.7 μm). Lateral size measurements of 120 EG sheets reveal that over 80% of the

EG sheets are larger than 5.0 μm (Figure 3b), and the largest flake size observed is ~44.0 μm (Supplementary Figure S7b). A histogram of flake thickness acquired across EG flakes using AFM shows a mean thickness of ~0.72 nm (Figure 3c), confirming the monolayer nature, which is comparable with the thickness of pristine graphene on a Si wafer.[25] The measured thickness of a bilayer and a multilayer ($\geq$4 layers) EG is 1.30 and 3.11 nm, respectively (Supplementary Figure S8). The thickness distribution of more than 50 sheets calculated from the AFM height profile is presented in Figure 3d. Remarkably, more than 85% of EG nanosheets comprise thin graphene ($\leq$3 layers), where single and bilayer graphenes are the dominant products (together ~72%). High-resolution transmission electron microscopic (HRTEM) images further disclose that the EG sheets range from a single layer to four layers (Figure 3e and Supplementary Figure S9). The selected area electron diffraction (SAED) pattern in Figure 3f exhibits a typical 6-fold symmetric diffraction with stronger diffraction from the (1-210) plane than from the (0-110) plane, indicating the high crystallinity of a bilayer graphene sheet.[13,26]

We then used Raman spectroscopy to identify defects in the graphene.[27,28] We performed Raman spectroscopy and mapping with a 532 nm excitation laser on EG deposited on SiO_2/Si substrates. Raman mapping of D and G peaks from a few-layer EG sheet (2−4 layers; selected layers are shown in Figure 4a) was extracted and plotted in Figure 3b and c, respectively. The D peak (~1350 cm^{-1}) was caused by the breathing mode of the sp^2 carbon atoms and activated by the existence of defects such as edges, functional groups, or structural disorders.[29] The intensity contrast in the color scale in Figure 4b and c shows that the intensity of the G peak is more than two times that of D peak (mean I_D/I_G ratio = 0.42), indicating a low degree of defects. The corresponding Raman
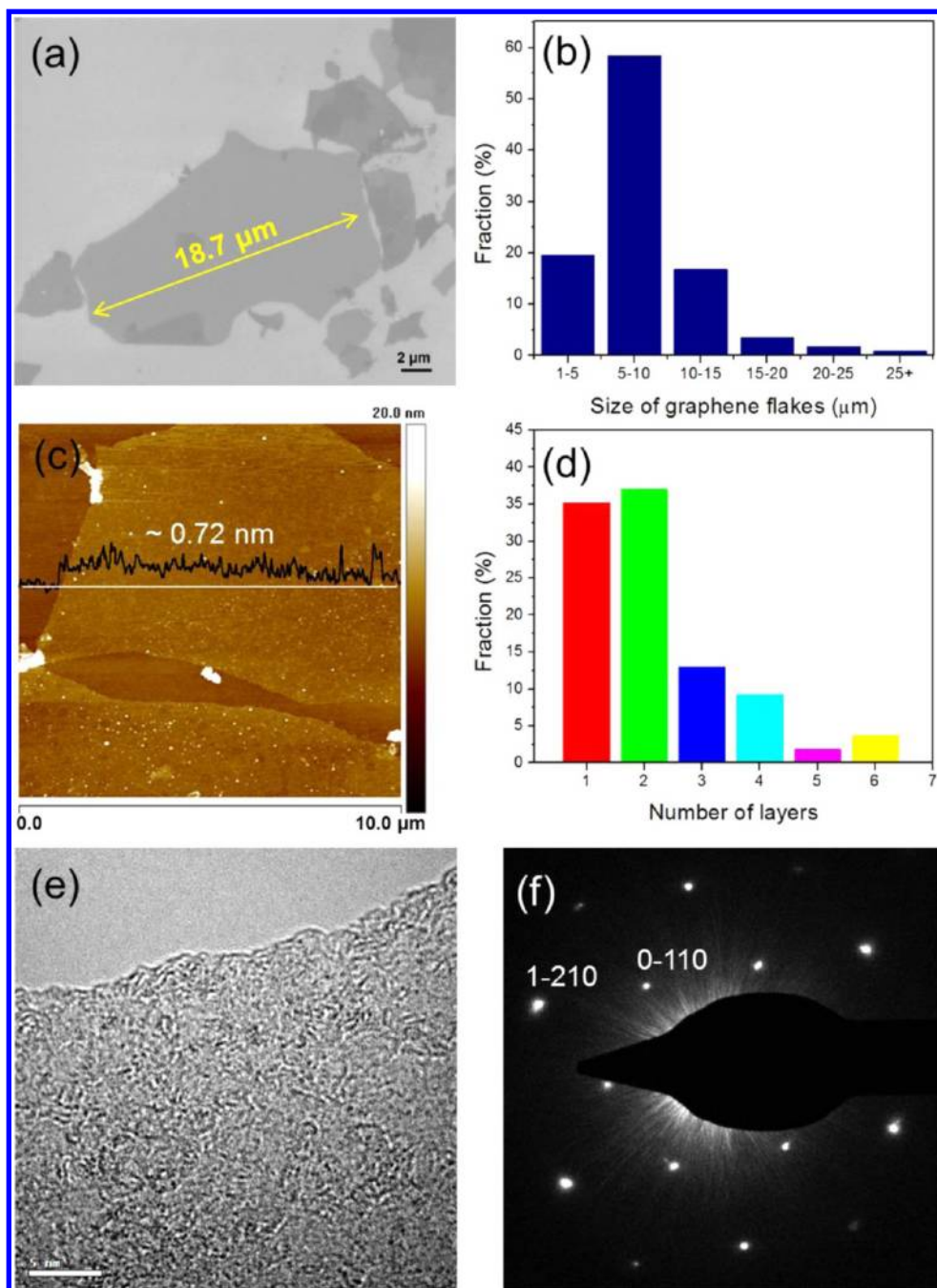
Figure 3. (a) SEM image of EG. (b) Statistical flake size analysis of graphene sheets by SEM., (c) AFM image of EG on silicon substrate. (d) Statistical thickness analysis of EG by AFM. (e) HRTEM of single-layer graphene. (f) SAED pattern of EG.

spectra in Figure 4d (measured near the center of the graphene flake) demonstrates an I_D/I_G ratio of 0.25, which is much smaller than for chemically or thermally reduced GO (~1.1–1.5)[30] and electrochemically exfoliated graphene (0.4) in acidic solution.[15]

X-ray photoelectron spectroscopy (XPS) was used to probe the chemical composition of the as-prepared EG. The EG showed approximately 5.5 atom % oxygen content on graphene (Supplementary Figure S10), which was much lower than that obtained in acidic electrolyte solution (i.e., 7.5 atom %).[15] Despite the presence of a tiny amount of oxygen originating from the oxidation of graphite by OH⁻ ions during the electrochemical process, the C/O ratio of 17.2 for EG was significantly higher than those reported for EG and rGO.[15,31,32]

A detailed comparison of the C/O ratios between rGO and different types of exfoliated graphene is presented in Supplementary Table S2. The deconvoluted XPS spectra of the C 1s peak (Figure 5a) disclose the presence of 3.64 atom % of C−OH (285.5 eV), 0.38 atom % of C═O (287.6 eV), and 1.48 atom % of C(O)−O (290.1 eV) groups.

Further structural analysis of EG by ¹³C magic angle spinning (MAS) NMR revealed a broad signal centered at 122 ppm (graphitic, C sp²), indicating the presence of pure sp² hybridized carbon sites (Supplementary Figure S11). In contrast, the NMR spectrum of GO showed an additional signal of sp³ hybridized carbons bound to oxygen (C−OH or C−O−C) in the range of 60–70 ppm. The signal of EG at 122 ppm was quite broad when compared to that of GO. This can
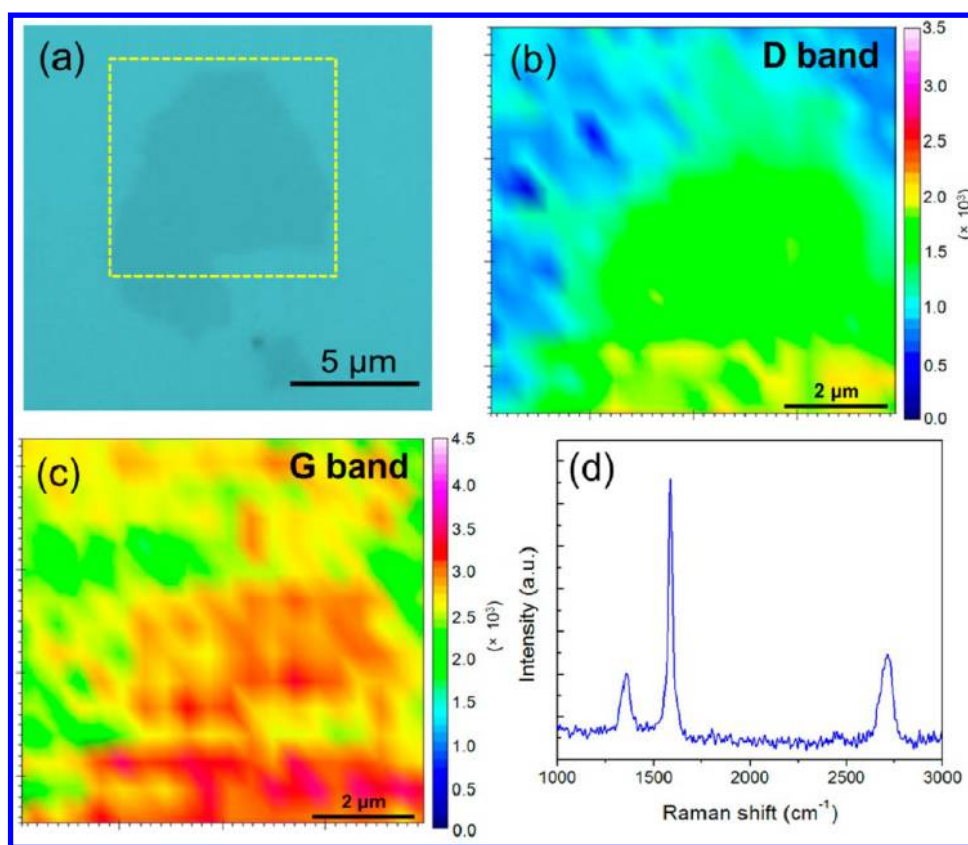
Figure 4. (a) Optical microscopic image of an EG flake. Scale bar 5 μm. (b, c) Raman intensity maps for D and G peaks, respectively. (d) Representative Raman spectra. The Raman excitation laser wavelength is 532 nm.
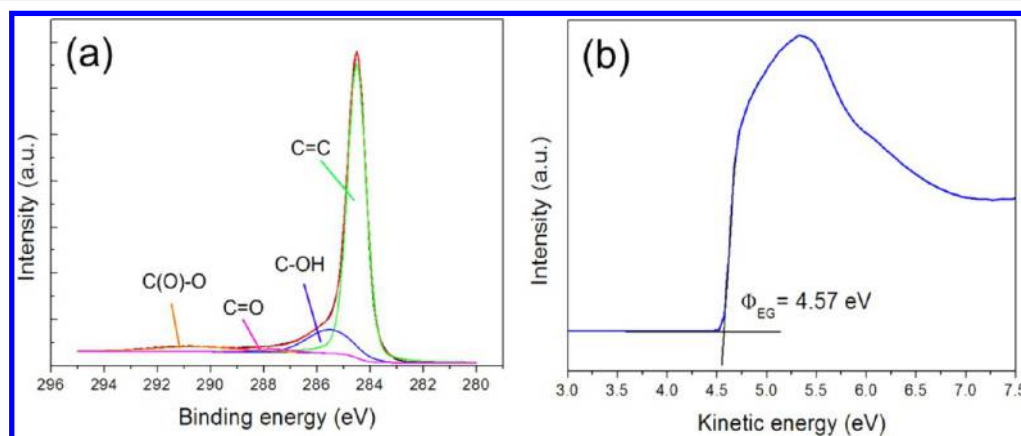
Figure 5. (a) XPS C 1s spectra of EG. (b) The secondary electron cutoff of EG measured from ultraviolet photoemission spectra.

be attributed to the high conductivity of EG, resulting in a higher number of perturbing magnetic moments of the free charges. The spinning of the EG sample in the magnetic field was difficult because of the high conductivity, which also limited the filling of MAS rotors.

The powder X-ray diffraction pattern of EG displayed a peak at 26.3° (d-spacing 3.48 Å; Supplementary Figure S12). The presence of a small amount of functional groups in EG acts as a spacer between layers and results in a lower 2θ angle with large d-spacing compared to that of graphite (26.5°, d-spacing ~3.36 Å), but significantly higher than rGO (25.0°, d-spacing ~3.56 Å).[31] Figure 5b displays the ultraviolet photoelectron spectra around the secondary-electron threshold region for a thin film of EG. The measured work function (Φ_{EG}) of EG was 4.57 eV,

slightly higher than that of pristine graphene (~4.50 eV).[33] This can be attributed to the presence of oxygen-containing functional groups in EG that can produce surface dipoles via the extraction of π electrons from graphene.[34]

Electronic Properties of EG. To examine the electronic properties of the as-prepared EG flakes, we fabricated field-effect transistor (FET) devices based on a thin EG film (thickness ~0.7–4 nm) and a single-layer EG sheet (thickness ~0.71 nm), respectively (Supplementary Figure S13). Both the thin EG film and isolated single-layer EG on SiO$_2$/Si substrates were prepared by using the Langmuir–Blodgett technique. The detailed device fabrication is described in the Supporting Information. The transfer curves of the FET devices based on the thin EG film and single-layer EG are presented in Figure 6a
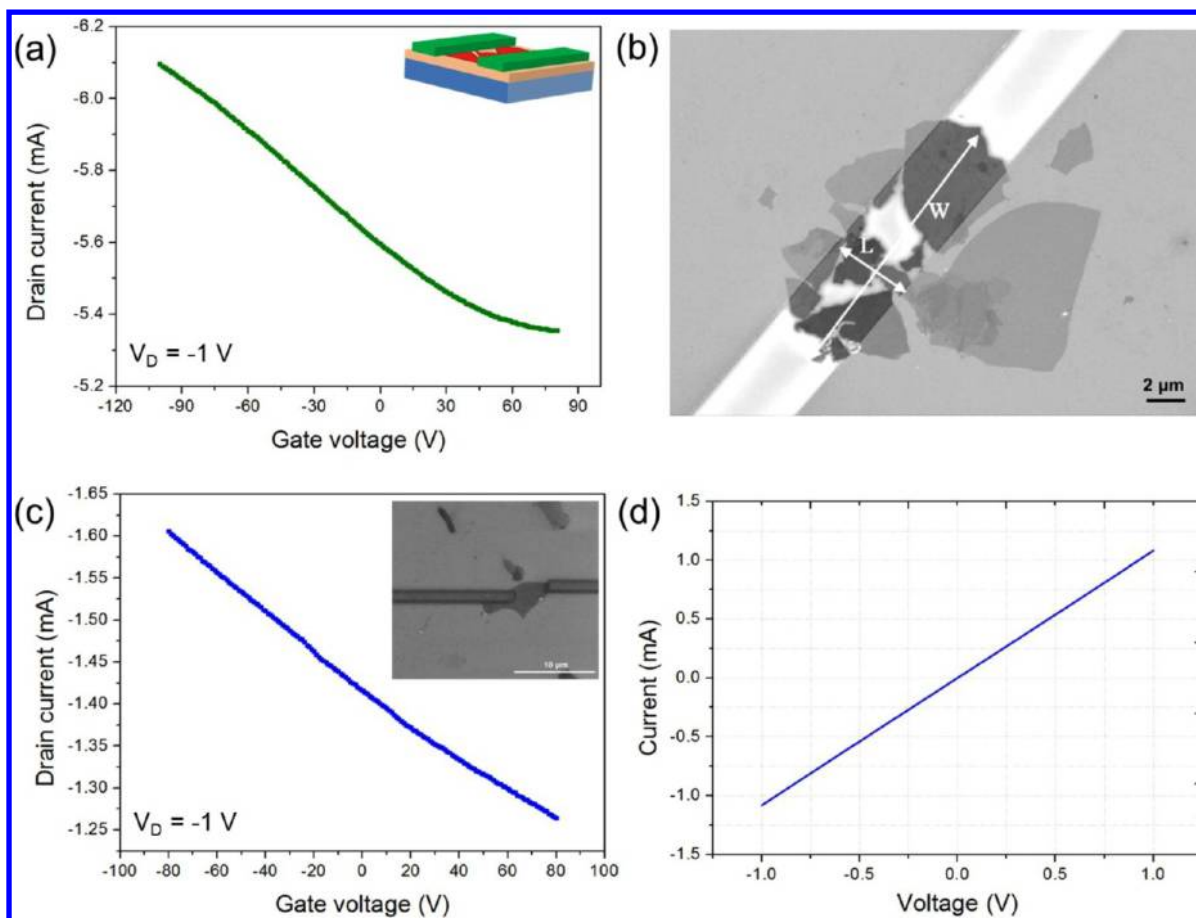
Figure 6. (a) Transfer curve for a FET device based on an EG thin film. (b) SEM image of the fabricated device showing thin EG flakes between the Au electrodes. Channel length and width are indicated by arrows. (c) Transfer curve of a FET device based on single-layer EG (inset is the SEM image of the fabricated device). (d) Current−voltage (I−V) curve of an isolated single-layer EG flake.

and c, respectively. Notably, the device based on the thin EG film (Figure 6a,b) possesses a maximum hole mobility of 98.2 cm^2 V^{-1} s^{-1}, whereas single-layer EG (Figure 6c) gives an excellent hole mobility of ∼310 cm^2 V^{-1} s^{-1} and a sheet resistance of 1.96 $k\Omega$ sq^{-1} (Figure 6d), comparable with undoped CVD-grown graphene (1.05 $k\Omega$ sq^{-1}).[35] The lower mobility of the thin film device can be attributed to the interjunction resistance between EG flakes. It should be emphasized that the hole mobility of single-layer EG achieved in this work is significantly higher than that of chemically reduced GO (123 cm^2 V^{-1} s^{-1})[31] or electrochemically exfoliated graphene in acidic solution (233 cm^2 V^{-1} s^{-1})[15] (see Supplementary Table S3 for detailed comparison).

EG Thin Films on Plastic Substrate. The high quality and solution-processability of EG allow for fabricating transparent graphene films on flexible poly(ethylene terephthalate) (PET) substrates by a vacuum filtration and dry transfer method (Supplementary Figure S14a).[15] Briefly, an EG dispersion of 0.1 mg mL^{-1} in DMF was vacuum-filtered through a poly(tetrafluoroethylene) (PTFE) membrane followed by mechanically pressing the filtered film against a PET substrate. Afterward, the PTFE membrane was peeled off, leaving the transferred EG film on the substrate due to van der Waals interaction between the substrate and graphene. The thickness of the transferred EG film could be adjusted by controlling the filtration volume and the concentration of EG dispersions. For example, vacuum filtration of 3 and 9 mL of EG dispersions

resulted in ∼6.0 and ∼16.0 nm graphene films on PET with ∼91% and ∼80% transparency, respectively (Supplementary Figure S14b). The sheet resistance (R_s) measured by a four-point probe system revealed a mean value of 24.2 and 7.56 $k\Omega$ sq^{-1} for 6.0 and 16.0 nm films, respectively. Low temperature annealing (i.e., 300 °C) of the EG films decreased the R_s to 7.61 and 1.81 $k\Omega$ sq^{-1}, respectively (Supplementary Figure S14c). Remarkably, further doping the EG films with 65% HNO_3 for 2 h led to R_s values of 0.87 and 0.33 $k\Omega$ sq^{-1}, respectively, without sacrificing the original transparency (Supplementary Figure S15).

EG Ink-Coated Paper for Flexible Supercapacitors. We further demonstrated the use of EG as conductive ink, which is an important requirement for next-generation printable electronics. Toward this end, a conductive graphene ink was prepared by dispersing EG flakes in DMF with a high concentration (10 mg mL^{-1}; Figure 7a). Application of the as-prepared graphene ink on A4-size paper using a paintbrush (Figure 7b) easily transformed the paper into an electrically conductive sheet. The bonding of cellulose fiber in paper produces many air passages or pores throughout the paper (Supplementary Figure S16a). Thus, the highly porous nature of paper provides a strong capillary force for the EG ink, enhancing solvent absorption and leading to a conformal coating of EG ink on paper (Supplementary Figure S16b). Moreover, a simple film adhesion test with a piece of cellophane tape demonstrated strong adhesion between the
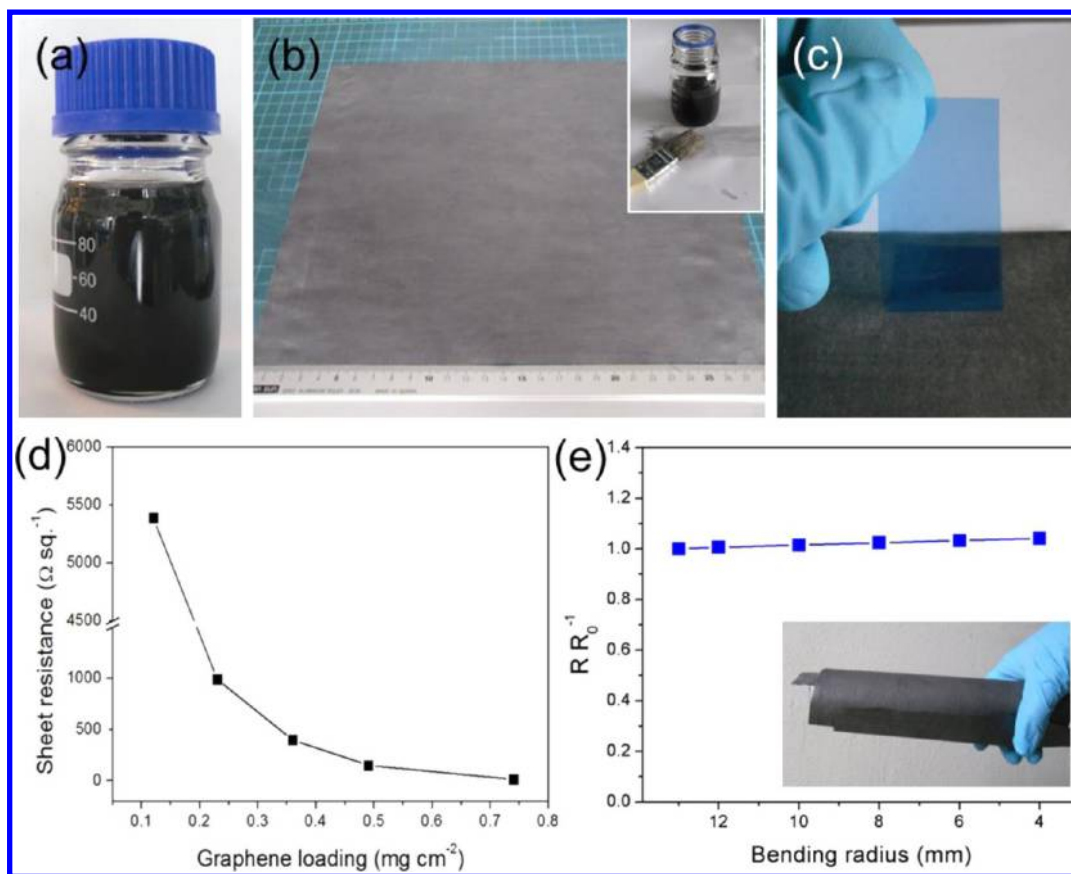
Figure 7. (a) Photograph of EG in DMF (10 mg mL^{-1}) used as an ink. (b) Commercial A4-size paper coated with EG using a paintbrush (inset). (c) Film adhesion test with cellophane tape. (d) Relationship between the resistances of the paper with graphene loading. (e) Changes in sheet resistance after bending the conductive paper into different radii.

EG and paper, confirming high film stability against damage, such as scratching or peeling off (Figure 7c). Figure 7d presents the relationship between the paper resistance and the amount of EG loading (in mg cm^{-2}). A sheet resistance of ~11 Ω sq^{-1} was obtained with an EG loading of 0.74 mg cm^{-2}, comparable to carbon nanotube paper.[36] Moreover, the graphene paper possessed excellent mechanical properties since after bending to a 4 mm radius there was no significant change in electrical conductivity (Figure 7e).

To demonstrate the multifunction of the EG paper, we explored the potential of EG-coated paper for all solid-state flexible supercapacitors. For this purpose, a poly(vinyl alcohol)/H$_2$SO$_4$ gel was drop-cast onto the top surface of EG-coated paper (with a loading of ~0.60 mg cm^{-2}) and solidified overnight. Afterward, two pieces of EG paper electrodes were integrated into an all-solid-state supercapacitor without using an additional current collector (Figure 8a). The electrochemical properties of the as-fabricated device were investigated by cyclic voltammetry. The binder- and additive-free fabricated EG paper-based supercapacitor exhibited typical double-layer capacitive behavior at various scan rates (Figure 8b,c). The area capacitance of the flexible EG paper supercapacitor was ~11.3 mF cm^{-2} at a low scan rate of 1 mV s^{-1} (Figure 8d), comparable to or even higher than that of thin-film rGO or carbon nanotubes on flexible substrates.[37,38] In addition, the gravimetric capacitance calculated on the basis of the area capacitance ranges from 18.8 to 56.6 F g^{-1}, depending of the loading of EG on paper varying from 0.6 to 0.2 mg cm^{-2}, respectively (Supplementary Figure S17). Remarkably, the

device exhibited high rate capability that could be operated up to 5000 mV s^{-1} (Figure 8c). The rate capability achieved in this work was thus superior to that of carbon nanotubes and/or rGO-coated cellulose paper supercapacitors.[37,39−42]

■ CONCLUSION

Taken together, our electrochemical exfoliation of graphite in aqueous sulfate salt electrolyte solution effectively reduces the oxidation degree and thereby significantly improves the chemical and electronic properties of graphene. Thin-layer graphene sheets were obtained at a high yield with large flake size and could be produced on a scale of tens of grams, demonstrating the great potential for industrial scale-up production. The EG has the highest C/O ratio (17.2) and hole mobility (~310 cm^2 V^{-1} s^{-1}) among all the reported values of EG obtained in acidic electrolytes and solution-processed rGO. The solution-processability of high-quality EG in organic solvents permits their direct use in transparent films and conductive ink, providing great advantage for the fabrication of graphene-based materials and devices. Low-cost and environmentally friendly production of such high-quality graphene is important, not only for future generation electronics but also for large-scale applications, such as composite materials, supercapacitors, fuel-cells, and batteries.

■ ASSOCIATED CONTENT

ⓈSupporting Information

Experimental details, photographs of electrochemical exfoliation on large scale and in different electrolyte systems, AFM,
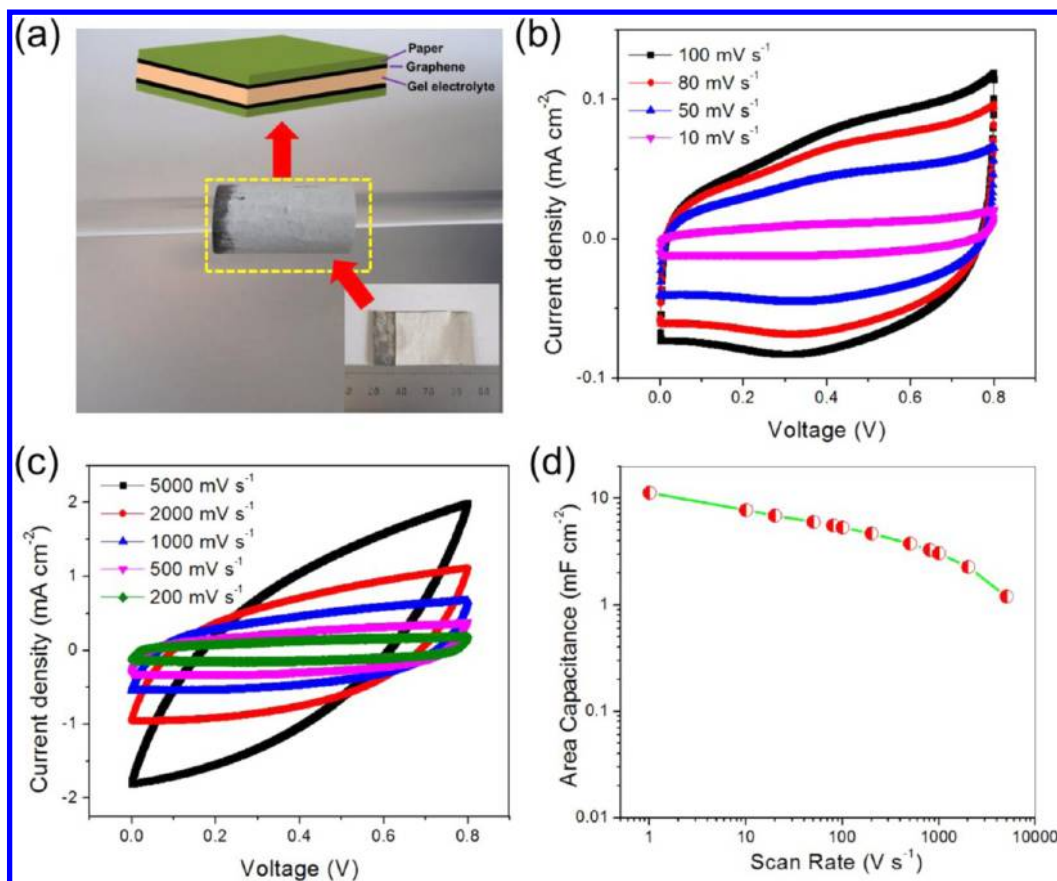
Figure 8. (a) Photographs of supercapacitor based on EG ink-coated paper, where the device is rolled around a glass rod. Inset shows a photograph of the device prior to rolling. (b and c) Cyclic voltammetry curves of EG paper-based supercapacitor (loading 0.6 mg cm^{-2}) at scan rates from 10 to 100 mV s^{-1} and 200 to 5000 mV s^{-1}, respectively. (d) Evolution of area capacitance versus scan rate.

HRTEM and optical microscopic images, XPS, solid-state NMR spectra and XRD of EG; AFM image of EG FET device; UV−vis and sheet resistance of EG thin film before and after acid doping; SEM image of EG-coated paper and electrochemical characterizations of EG paper-based supercapacitors; summary of electrochemical exfoliation in different inorganic salts; and comparison of elemental analysis and mobility of EG with different types of graphene. This material is available free of charge via the Internet at http://pubs.acs.org.

■ AUTHOR INFORMATION

Corresponding Authors
feng@mpip-mainz.mpg.de
muellen@mpip-mainz.mpg.de

Notes
The authors declare no competing financial interest.

■ REFERENCES

(1) Wang, Y.; Chen, X.; Zhong, Y.; Zhu, F.; Loh, K. P. *Appl. Phys. Lett.* **2009**, *95*, 063302.
(2) Bae, S.; Kim, H.; Lee, Y.; Xu, X. F.; Park, J. S.; Zheng, Y.; Balakrishnan, J.; Lei, T.; Kim, H. R.; Song, Y. I.; Kim, Y. J.; Kim, K. S.; Ozyilmaz, B.; Ahn, J. H.; Hong, B. H.; Iijima, S. *Nat. Nanotechnol.* **2010**, *5*, 574.
(3) Wu, D. Q.; Zhang, F.; Liang, H. W.; Feng, X. L. *Chem. Soc. Rev.* **2012**, *41*, 6160.
(4) Parvez, K.; Yang, S. B.; Hernandez, Y.; Winter, A.; Turchanin, A.; Feng, X. L.; Müllen, K. *ACS Nano* **2012**, *6*, 9541.
(5) Wu, Z. S.; Parvez, K.; Feng, X.; Müllen, K. *Nat. Commun.* **2013**, *4*, 2487.
(6) Geim, A. K.; Novoselov, K. S. *Nat. Mater.* **2007**, *6*, 183.
(7) Park, S.; Ruoff, R. S. *Nat. Nanotechnol.* **2009**, *4*, 217.
(8) Novoselov, K. S.; Geim, A. K.; Morozov, S. V.; Jiang, D.; Zhang, Y.; Dubonos, S. V.; Grigorieva, I. V.; Firsov, A. A. *Science* **2004**, *306*, 666.
(9) Sutter, P. W.; Flege, J. I.; Sutter, E. A. *Nat. Mater.* **2008**, *7*, 406.
(10) Lee, Y.; Bae, S.; Jang, H.; Jang, S.; Zhu, S. E.; Sim, S. H.; Song, Y. I.; Hong, B. H.; Ahn, J. H. *Nano Lett.* **2010**, *10*, 490.
(11) Eda, G.; Fanchini, G.; Chhowalla, M. *Nat. Nanotechnol.* **2008**, *3*, 270.
(12) Hernandez, Y.; Nicolosi, V.; Lotya, M.; Blighe, F. M.; Sun, Z. Y.; De, S.; McGovern, I. T.; Holland, B.; Byrne, M.; Gun'ko, Y. K.; Boland, J. J.; Niraj, P.; Duesberg, G.; Krishnamurthy, S.; Goodhue, R.; Hutchison, J.; Scardaci, V.; Ferrari, A. C.; Coleman, J. N. *Nat. Nanotechnol.* **2008**, *3*, 563.
(13) Wang, J. Z.; Manga, K. K.; Bao, Q. L.; Loh, K. P. *J. Am. Chem. Soc.* **2011**, *133*, 8888.
(14) Shih, C. J.; Vijayaraghavan, A.; Krishnan, R.; Sharma, R.; Han, J. H.; Ham, M. H.; Jin, Z.; Lin, S. C.; Paulus, G. L. C.; Reuel, N. F.; Wang, Q. H.; Blankschtein, D.; Strano, M. S. *Nat. Nanotechnol.* **2011**, *6*, 439.
(15) Parvez, K.; Li, R. J.; Puniredd, S. R.; Hernandez, Y.; Hinkel, F.; Wang, S. H.; Feng, X. L.; Müllen, K. *ACS Nano* **2013**, *7*, 3598.

(16) Lee, J. H.; Shin, D. W.; Makotchenko, V. G.; Nazarov, A. S.; Fedorov, V. E.; Kim, Y. H.; Choi, J. Y.; Kim, J. M.; Yoo, J. B. *Adv. Mater.* **2009**, *21*, 4383.

(17) Liu, N.; Luo, F.; Wu, H. X.; Liu, Y. H.; Zhang, C.; Chen, J. *Adv. Funct. Mater.* **2008**, *18*, 1518.

(18) Su, C. Y.; Lu, A. Y.; Xu, Y. P.; Chen, F. R.; Khlobystov, A. N.; Li, L. J. *ACS Nano* **2011**, *5*, 2332.

(19) Lu, J.; Yang, J. X.; Wang, J. Z.; Lim, A. L.; Wang, S.; Loh, K. P. *ACS Nano* **2009**, *3*, 2367.

(20) Liu, J. L.; Yang, H. P.; Zhen, S. G.; Poh, C. K.; Chaurasia, A.; Luo, J. S.; Wu, X. Y.; Yeow, E. K. L.; Sahoo, N. G.; Lin, J. Y.; Shen, Z. X. *RSC Adv.* **2013**, *3*, 11745.

(21) Shang, N. G.; Papakonstantinou, P.; Sharma, S.; Lubarsky, G.; Li, M. X.; McNeill, D. W.; Quinn, A. J.; Zhou, W. Z.; Blackley, R. *Chem. Commun.* **2012**, *48*, 1877.

(22) Beck, F.; Jiang, J.; Krohn, H. *J. Electroanal. Chem.* **1995**, *389*, 161.

(23) Beck, F.; Junge, H.; Krohn, H. *Electrochim. Acta* **1981**, *26*, 799.

(24) Goss, C. A.; Brumfield, J. C.; Irene, E. A.; Murray, R. W. *Anal. Chem.* **1993**, *65*, 1378.

(25) Cheng, Z. G.; Zhou, Q. Y.; Wang, C. X.; Li, Q. A.; Wang, C.; Fang, Y. *Nano Lett.* **2011**, *11*, 767.

(26) Sun, Z. Z.; Yan, Z.; Yao, J.; Beitler, E.; Zhu, Y.; Tour, J. M. *Nature* **2010**, *468*, 549.

(27) Yu, Q. K.; Jauregui, L. A.; Wu, W.; Colby, R.; Tian, J. F.; Su, Z. H.; Cao, H. L.; Liu, Z. H.; Pandey, D.; Wei, D. G.; Chung, T. F.; Peng, P.; Guisinger, N. P.; Stach, E. A.; Bao, J. M.; Pei, S. S.; Chen, Y. P. *Nat. Mater.* **2011**, *10*, 443.

(28) Malard, L. M.; Pimenta, M. A.; Dresselhaus, G.; Dresselhaus, M. S. *Phys. Rep.* **2009**, *473*, 51.

(29) Ferrari, A. C.; Meyer, J. C.; Scardaci, V.; Casiraghi, C.; Lazzeri, M.; Mauri, F.; Piscanec, S.; Jiang, D.; Novoselov, K. S.; Roth, S.; Geim, A. K. *Phys. Rev. Lett.* **2006**, *97*, 187401.

(30) Buglione, L.; Chng, E. L. K.; Ambrosi, A.; Sofer, Z.; Pumera, M. *Electrochem. Commun.* **2012**, *14*, 5.

(31) Feng, H.; Cheng, R.; Zhao, X.; Duan, X.; Li, J. *Nat. Commun.* **2013**, *4*, 1539.

(32) Moon, I. K.; Lee, J.; Ruoff, R. S.; Lee, H. *Nat. Commun.* **2010**, *1*, 73.

(33) Shin, H. J.; Choi, W. M.; Choi, D.; Han, G. H.; Yoon, S. M.; Park, H. K.; Kim, S. W.; Jin, Y. W.; Lee, S. Y.; Kim, J. M.; Choi, J. Y.; Lee, Y. H. *J. Am. Chem. Soc.* **2010**, *132*, 15603.

(34) Li, S. S.; Tu, K. H.; Lin, C. C.; Chen, C. W.; Chhowalla, M. *ACS Nano* **2010**, *4*, 3169.

(35) Kholmanov, I. N.; Magnuson, C. W.; Aliev, A. E.; Li, H. F.; Zhang, B.; Suk, J. W.; Zhang, L. L.; Peng, E.; Mousavi, S. H.; Khanikaev, A. B.; Piner, R.; Shvets, G.; Ruoff, R. S. *Nano Lett.* **2012**, *12*, 5679.

(36) Hu, L.; Choi, J. W.; Yang, Y.; Jeong, S.; La Mantia, F.; Cui, L. F.; Cui, Y. *Proc. Natl. Acad. Sci. U.S.A.* **2009**, *106*, 21490.

(37) Yoo, J. J.; Balakrishnan, K.; Huang, J. S.; Meunier, V.; Sumpter, B. G.; Srivastava, A.; Conway, M.; Reddy, A. L. M.; Yu, J.; Vajtai, R.; Ajayan, P. M. *Nano Lett.* **2011**, *11*, 1423.

(38) Kaempgen, M.; Chan, C. K.; Ma, J.; Cui, Y.; Gruner, G. *Nano Lett.* **2009**, *9*, 1872.

(39) Hu, S.; Rajamani, R.; Yu, X. *Appl. Phys. Lett.* **2012**, *100*, 104103.

(40) Weng, Z.; Su, Y.; Wang, D. W.; Li, F.; Du, J. H.; Cheng, H. M. *Adv. Energy Mater.* **2011**, *1*, 917.

(41) Kang, Y. J.; Chun, S. J.; Lee, S. S.; Kim, B. Y.; Kim, J. H.; Chung, H.; Lee, S. Y.; Kim, W. *ACS Nano* **2012**, *6*, 6400.

(42) Kang, Y. J.; Chung, H.; Han, C. H.; Kim, W. *Nanotechnology* **2012**, *23*, 065401.